RESEARCH ARTICLE
doi: 10.2306/scienceasia1513-1874.2026.004

ScienceAsia 51 (6): 2025: ID 2026004: **1–9**

Imperatorin alleviates cancer cell viability by suppressing M2 macrophage polarization through Nox2-ROS signaling pathway

Suyun Yong[a], **Jianhua Wang**[b], **Nan Zhou**[a,*], **Peng Zhang**[a]

[a] Department of Pharmacy, Shaanxi Provincial People's Hospital, Xi'an, Shaanxi 710068 China
[b] Second Department of General Surgery, Shaanxi Provincial People's Hospital, Xi'an, Shaanxi 710068 China

*Corresponding author, e-mail: zhounansx2024@163.com

Received 28 May 2025, Accepted 8 Dec 2025
Available online 15 Jan 2026

ABSTRACT: The tumor microenvironment (TME) plays a crucial role in regulating tumor progression. Tumor-associated macrophages, as prominent cellular components of the tumor microenvironment, exhibit high plasticity and can either promote or suppress tumor development. Imperatorin, a natural coumarin derivative with diverse pharmacological activities, has been reported to inhibit vascular remodeling and cancer progression. In this study, we aimed to explore the potential mechanisms by which imperatorin regulates TME in colon cancer cells. A co-culture model of macrophages with colon cancer HT-29 and LoVo cells was established and treated with imperatorin. CCK-8 assay was used to measure cell viability. M2 macrophage surface markers were determined by immunohistochemistry and enzyme-linked immunosorbent assay. ROS level was measured through Dihydroethidium fluorescent probe assay. The mRNA and protein expression of nicotinamide adenine dinucleotide phosphate oxidase were detected by RT-PCR and Western blot analysis. Treatment with imperatorin effectively decreased the viability of the colon cancer HT-29 and LoVo cells, inhibited the cytokine CSF-1 which induced upregulation of CD163 and CD206 in macrophages, and reduced the expression of M2 macrophage phenotype markers and the Nox2/ROS/AMPK/STAT3 signaling pathway. These results suggest that imperatorin inhibits M2 macrophage polarization and attenuates the viability of colon cancer HT-29 and LoVo cells by downregulating the expression of the Nox2/ROS/AMPK/STAT3 signaling pathway.

KEYWORDS: imperatorin, tumor-associated macrophages, tumor microenvironment, NADPH oxidases, reactive oxygen species

INTRODUCTION

According to GLOBOCAN 2020, the cancer burden is projected to increase by 47% by 2040 compared with 2020, with the number of new cancer cases reaching approximately 28.4 million [1]. Cancer development is regulated by multiple factors. Growing evidence indicates that the tumor microenvironment (TME) plays a key role in tumor progression and targeting the TME may represent an important strategy for cancer therapy [2]. TME is a highly heterogeneous and dynamic nature system, in which the immunosuppressive properties of TME enable tumor cells to achieve immune escape and promote the development of malignant tumors. Tumor-associated macrophages (TAM) are the most abundant immune cells in the TME and play a crucial role in tumor immune escape. Macrophages can be polarized into two major phenotypes: pro-inflammatory (M1) and anti-inflammatory (M2) phenotypes. Activation of toll-like receptors promotes the differentiation of tumor-associated macrophages into the M1 phenotype. M1 macrophages secrete pro-inflammatory cytokines such as tumor necrosis factor-α (TNF-α) and interleukin-1 (IL-1), which enhance T-cell function and inhibit the proliferation of tumor cells. In contrast, cytokines such as macrophage-colony stimulating factor (CSF-1) can induce TAM to polarize into M2 macrophages and release anti-inflammatory cytokines, including IL-10, IL-6, transforming growth factor β (TGF-β), and arginase 1 (ARG1), which inhibit T-cell function and promote tumor growth. TAM usually exhibits an M2-like function. TME is characterized by hypoxia, nutrient deficiencies, and extracellular low pH regions [3–5]. Reoxygenation and cell proliferation following cycling hypoxia can lead to reactive oxygen species (ROS) production [6]. ROS plays a key role in regulating the TME pathway, and modulation of ROS levels to reverse drug resistance in cancer cells without compromising normal cell function may represent a promising therapeutic strategy [7]. ROS is mainly produced by nicotinamide adenine dinucleotide phosphate (NADPH) oxidases (Noxs). The Nox family has seven members, namely Nox1-5, Dual oxidase1 (DUOX1), and Dual oxidase2 (DUOX2). Nox protein catalytic activity requires the association with a variety of subunits to form stable complexes, including p22Phox, p47Phox (isomer NoxO1), p67Phox (isomer NoxA1), and p40Phox [8, 9]. Nox2, which is found in the plasma membrane of phagocytes, is the main source of ROS in TAM [10]. Nox2-induced production of ROS enables macrophage polarization to M2 TAM during tumor development, promoting angiogenesis, tumor growth, and metastasis [11]. Therefore, targeting Nox2 may be an important strategy for modulating TME and inhibiting tumor progression.

Imperatorin (IMP) belongs to the furanocoumarin class, and studies have shown that imperatorin mainly exhibits antitumor and anti-inflammatory activities [12, 13]. In recent studies, imperatorin reduced H2O2-induced cell death in human hepatocellular carcinoma (HepG2) cells and attenuated ROS levels without cytotoxicity [14]. In addition, IMP may reduce ROS production and decrease inflammatory responses by downregulating nuclear factor erythroid 2-related factor 2 (Nrf2)/heme oxygenase-1 (HO-1) ROS/phosphoinositide 3-kinase (PI3K) protein kinase B (Akt), Nrf2/HO-1/ROS/mitogen-activated protein kinase (MAPK) and Nrf2/HO-1/ROS/nuclear factor kappa-B (NFκB) pathways [15]. These studies suggest that the multiple pharmacological effects of IMP may be closely associated with its ability to inhibit ROS levels. Previous studies from our group have confirmed that administration of IMP can both inhibit the proliferation of human gastric cancer MKN-45 cells and human colon cancer HT-29 cells, as well as reduce the levels of Noxs and ROS [16]. The above research indicates that IMP can regulate TME, and its pharmacological mechanism is closely related to Noxs. However, the antitumor mechanism of IMP is still unclear. This study aims to explore the potential effects and mechanisms by which IMP regulates the TME in colon cancer cells through a macrophage differentiation model, providing a possible therapeutic application for IMP in modulating the TME.

MATERIALS AND METHODS

Chemicals and reagents

Imperatorin and diphenyleneiodonium chloride were purchased from MedChemExpress (New Jersey, USA). RIPA lysis buffer, bicinchoninic acid (BCA) protein assay kit, and reactive oxygen species assay kit were obtained from Beyotime Institute of Biotechnology (Shanghai, China). Roswell Park Memorial Institute (RPMI) 1640 medium was purchased from Procell Institute of Biotechnology (Wuhan, China). Fetal bovine serum was purchased from ExCell Bio (Shanghai, China). Ampicillin, streptomycin sulfate, and phenylmethanesulfonyl fluoride (PMSF) were purchased from Aladdin (Henan, China). Trizol was obtained from Thermo Fisher Scientific (Waltham, USA). HiScript II Q RT SuperMix for quantitative polymerase chain reaction (qPCR), HiScript II Q Select RT SuperMix for qPCR, and AceQ qPCR SYBR Green Master Mix were purchased from Vazyme (Nanjing, China). Taq Plus DNA Polymerase, DL2000 DNA Marker, and dNTPs were obtained from Tiangen (Beijing, China). CD163 and CD206 were obtained from Proteintech Group (Wuhan, China). IL-6, IL-10, and TGF-β1 were obtained from Jiangsu Meimian Industrial (Jiangsu, China). Phorbol-12-myristate-13-acetate (PMA) was purchased from Sigma-Aldrich (Darmstadt, Germany). Signal transducer and activator of transcription 3 (p-STAT3), HO-1, P47phox, and adenosine 5′-monophosphate-activated protein kinase (p-AMPK) were obtained from Affinity Biosciences (San Antonio, USA). ARG1, Nox2, P22phox, and P67phox were obtained from Abcam (Cambridge, UK). HRP-conjugated goat anti-rabbit IgG and Anti-GAPDH rabbit polyclonal antibody were obtained from Boster-bio (Wuhan, China).

Preparation of imperatorin (IMP)

IMP and diphenyleneiodonium chloride (DPI) were diluted to a concentration of 50 mg/ml with DMSO and stored at a temperature of −20 °C for further use. For use, the solution was diluted with the appropriate medium to achieve the desired concentration.

Human myeloid leukemia mononuclear cell (THP-1) culture and differentiation

THP-1 cells were purchased from Wuhan Huayan Biotechnology (Wuhan, China). Cells were maintained in Dulbecco's modified Eagle's medium (DMEM) supplemented with 100 U of penicillin per ml, 100 μg of streptomycin per ml, and 10% fetal bovine serum at 37 °C in a humidified atmosphere containing 5% CO_2. Cells were passaged at a 1:3 ratio when the cell confluence reached 80%. For THP-1 differentiation to macrophage, THP-1 cells were incubated at a density of 1×10^6 with PMA (100 ng/ml) for 24 h. The cells were divided into the following experimental groups: (1) control, cultured in DMEM for 72 h; (2) CSF-1 group, treated with CSF-1 (100 ng/ml) for 72 h; (3) CSF-1 + DPI group, treated with DPI (5 μM) for 24 h followed by CSF-1 (100 ng/ml) for 72 h; (4) CSF-1 + IMP group, treated with IMP (10 μM) for 24 h followed by CSF-1 (100 ng/ml) for 72 h.

Preparation of conditioned medium

The four groups of cells were collected, the medium was discarded, and the cells were washed three times with PBS. The cells were then incubated in serum-free medium for 48 h. The medium was collected and centrifuged at 1,000 rpm for 10 min. The supernatants were collected as conditioned medium (CM). The CM can be stored at −80 °C for a short period to preserve the integrity of factors released by macrophages.

Cell Counting Kit-8 (CCK-8) assay

HT-29 and LoVo cells were collected and seeded into 96-well plates at a density of 5×10^3 cells/well and cultured overnight at 37 °C in a 5% CO_2 incubator (100 μl of sterile PBS was gently added to the side of each well). The four groups of conditioned medium and complete medium were mixed thoroughly at a 1:1 concentration and then separately co-cultured with HT-29 and LoVo cells for 24 h and 72 h. Afterward, 10 μl of CCK-8 was added to each well, followed by incubation for 1–4 h at 37 °C. The absorbance at 450 nm (OD_{450}) of each well was measured using

a microplate reader. Cell viability = $(OD_{experiment} - OD_{blank})/(OD_{control} - OD_{blank})$.

Immunohistochemistry

Cells were collected and fixed with 4% paraformaldehyde for 15 min and permeabilized with 0.5% Triton X-100 (PBS) for 20 min at room temperature. Afterward, 3% hydrogen peroxide was added to block endogenous peroxidase. Then, coverslips were blocked with diluted goat serum for 30 min, and the sections were incubated with primary antibodies overnight at 4 °C; the primary antibodies were CD163 (1:100) and CD206 (1:100). The sections were washed with PBS three times (3 min each) and then incubated with anti-mouse/rabbit secondary antibodies conjugated to horseradish peroxidase (HRP) at 37 °C for 30 min. After washing, the cells were stained with 3,3 N-diaminobenzidine tetrahydrochloride (DAB), counterstained with hematoxylin, and dehydrated. The coverslips were observed under a microscope, and images were captured. For each image, the integrated optical density (IOD) and area (pixels) were measured, and the mean optical density (MOD = IOD/area) was calculated.

Enzyme-linked immunosorbent assay (ELISA)

Cells were collected and digested with 0.25% trypsin. After centrifugation, the cells were resuspended in 200 µl of PBS and fragmented by repeated freeze-thawing. Then, after centrifugation at 3,000 rpm for 10 min, supernatant was detected by 96-well ELISA plates. Standard wells and sample wells were prepared. Then, 50 µl of the corresponding solution was added into each standard well, and 40 µl of sample diluent was added to each sample well. Subsequently, 10 µl of the test sample was added to each sample well, followed by incubated at 37 °C for 30 min. Fifty microliters of detected antibodies were added to the 96-well plates and incubated at 37 °C for 30 min. After washing the plates five times, 50 µl of developer A and 50 µl of developer B were added to each well and incubated at 37 °C for 10 min in the dark. Afterward, 50 µl of stop solution was added to each well, and the absorbance at 450 nm was measured using a microplate reader.

Quantitative RT-PCR

Cells were collected, and RNA was extracted from tissues using TRIzol reagent. RNA was stored at −80 °C until further use. RNA was reverse-transcribed into complementary DNA (cDNA) using RT-PCR kits. The mRNA levels of Nox2, p22phox, p47phox, and p67phox in cells were quantified using SYBR green dye. The two-step PCR amplification program was as follows: pre-denaturation at 95 °C for 10 min, followed by 40 cycles at 95 °C for 15 s and 60 °C for 60 s. The $2^{-\Delta\Delta Ct}$ method was used to calculate the relative index of gene expression. The specific primer sequences used are listed in Table S1.

Measurement of ROS

Cells were collected and centrifuged. The supernatant was discarded, and the cell pellet was resuspended in PBS. Dihydroethidium (DHE), a commonly used fluorescent probe for detecting superoxide anions, enter cells and reacts with superoxide anions to produce red fluorescence, which is used for ROS detection. DHE was added at a final concentration of 0.5 µM and incubated for 1 h in the dark. After incubation, the cells were observed under a fluorescence microscope. The mean optical density (MOD) of ROS fluorescence was quantified using Image-Pro Plus 6.0 (IPP 6.0, Media Cybernetics, USA). For each image, the integrated optical density (IOD) and the corresponding area were measured, and MOD was calculated as IOD/area.

Western blot analysis

Cells were collected, placed on ice, and homogenized in cell lysis buffer. After centrifugation, the total protein concentration was determined using BCA assay. Approximately 20 µg of protein was loaded, separated by sodium dodecyl sulfate — polyacrylamide gel electrophoresis (SDS-PAGE), and transferred to polyvinylidene fluoride (PVDF) membrane, which was blocked with nonfat milk at room temperature for 2 h. The membrane was incubated with the primary antibodies at 4 °C overnight. The primary antibodies were glyceraldehyde-3-phosphate dehydrogenase (GAPDH) (1:1000), P-AMPK (1:1000), P-STAT3 (1:1000), HO-1 (1:1000), ARG1 (1:1000), Nox2 (1:5000), p22phox (1:1000), p47phox (1:1000), and p67phox (1:2000). After incubation, the membrane was washed three times with Rapid Blocking Buffer (TBST) and incubated with the secondary antibodies (1:10,000) at room temperature for 2 h. The protein bands were visualized using an ECL kit, and the band intensities were analyzed using Image-Pro Plus software.

Statistical analysis

Results are presented as mean ± standard error of the mean (SEM). When three or four groups were compared, one-way ANOVA followed by Tukey's multiple comparison test was used. Statistical significance was set at $p < 0.05$.

RESULTS

Attenuation of the colon cancer HT-29 and LoVo cell viability by IMP

We explored the role of IMP in colon cancer HT-29 and LoVo cells. To determine whether IMP could decrease the HT-29 and LoVo cell viability, PMA was used to induce THP-1 differentiation to M0 macrophages, and CSF-1 was used to promote M2 macrophage polarization. Subsequently, the conditioned medium from macrophage was co-cultured with HT-29 and LoVo

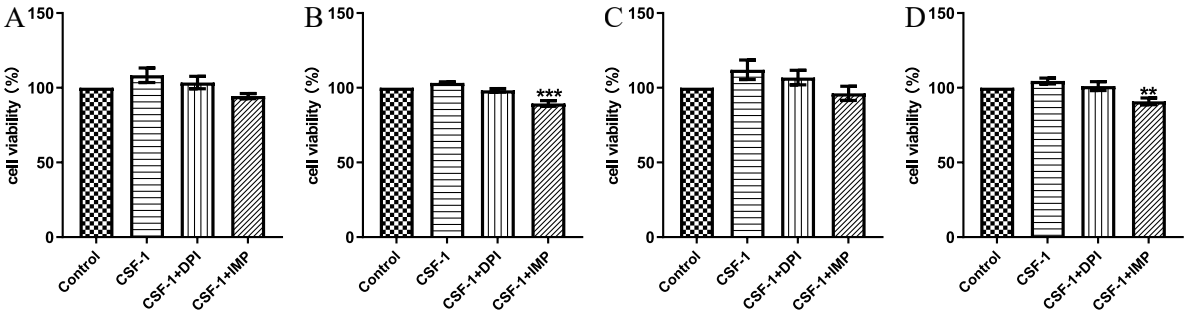

Fig. 1 Effect of IMP (10 μM) on the viability of colon cancer HT-29 and LoVo cells. CCK-8 assay used to determine the viability of HT-29 cells at 24 h (A) and 72 h (B) and LoVo cells at 24 h (C) and 72 h (D). ** $p < 0.01$ vs. CSF-1, *** $p < 0.001$ vs. CSF-1.

cells. As shown in Fig. 1, administration of IMP significantly reversed the CSF-1 induced increase in cell viability in both HT-29 and LoVo cells at 72 h (** $p < 0.01$, *** $p < 0.001$). IMP showed a reversal effect at 24 h, but the difference was not statistically significant. These results indicate that IMP inhibited HT-29 and LoVo cell viability via macrophage modulation.

Inhibition of CSF-1 induced increases in CD163 and CD206 expression levels in macrophages by IMP

To further clarify the role of IMP on the macrophages, we performed immunohistochemistry to detect the expression levels of M2 macrophage phenotype markers CD163 and CD206. As shown in Fig. 2, the expression levels of CD163 and CD206 were significantly increased in the CSF-1 intervention group compared with the control group (*** $p < 0.001$). Conversely, IMP and DPI interventions markedly inhibited these increases in the THP-1 cells (* $p < 0.05$, ** $p < 0.01$, *** $p < 0.001$). These results suggest that IMP decreases tumor viability toward inhibiting M2 macrophage polarization.

Attenuation of M2 macrophage phenotype marker expression levels by IMP

Next, we investigated the effect of IMP on M2 macrophage phenotype markers. ELISA was used to detect the expression levels of IL-10, IL-6, and TGF-β1, which are M2 macrophage phenotype markers. Fig. 3 showed that the expressions of IL-10, IL-6, and TGF-β1 were significantly increased compared with control group after administration of CSF-1 in THP-1 cells (*** $p < 0.001$), and the expression of these markers was significantly decreased by both IMP and DPI (** $p < 0.01$, *** $p < 0.001$).

Inhibition of CSF-1 induced Nox2 and ROS expression levels in macrophages by IMP

The effect of IMP on Nox2-associated mRNA and ROS expression was detected by PCR and DHE fluorescent probe assay (Fig. 4), and the results showed that CSF-1 intervention significantly increased the mRNA expression of Nox2, p22phox, p47phox, and p67phox in THP-1 cells compared with the control group (*** $p < 0.001$). Administration of IMP and DPI significantly reduced mRNA expression of Nox2, p22phox, p47phox, and p67phox (** $p < 0.01$, *** $p < 0.001$). The DHE fluorescent probe assay showed that compared with control, CSF-1 intervention significantly elevated the ROS level (*** $p < 0.001$). Administration of IMP and DPI decreased ROS levels in macrophages (*** $p < 0.001$).

Inhibition of Nox2/ROS/AMPK/STAT3 pathway expression levels in M2 macrophages by IMP

The effect of IMP on the expression of Nox2/ROS/AMPK/STAT3 pathway-associated proteins and the M2 macrophage markers HO-1 and ARG-1 was measured by Western-blot. The results showed that administration of CSF-1, the expression of Nox2, p22phox, p67phox, p47phox, p-AMPK, p-STAT3, HO-1 and ARG1 proteins was increased in comparison with control group (** $p < 0.01$, *** $p < 0.001$), and the expression levels of all proteins were significantly decreased after administration of IMP (* $p < 0.05$, ** $p < 0.01$). Administration of DPI also notably downregulated the protein expression level of p-STAT3 (* $p < 0.05$) (Fig. 5). Therefore, we conclude that IMP reduces the viability of HT-29 and LoVo cells through the Nox2/ROS/AMPK/STAT3 pathway.

DISCUSSION

IMP has multiple pharmacological effects such as antibacterial, anti-inflammatory, and antioxidant activities, making it a promising candidate drug. Its antitumor activity has attracted increasing attention from researchers [17]. However, most studies on imperatorin are limited to pharmacodynamic evaluations, and comprehensive, in-depth investigations systematically revealing its mechanisms and effective targets are lacking. In the present study, we explored the potential role of IMP in colon cancer, and our results show for the first time that treatment with IMP effectively inhibits M2 macrophage polarization and the proliferative ability

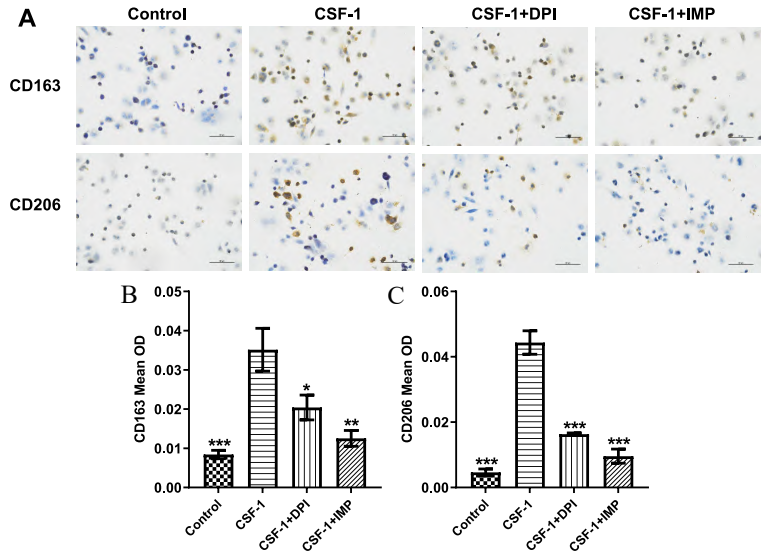

Fig. 2 Effect of IMP (10 μM) on the expression levels of M2 macrophage phenotype markers CD163 and CD206. Immunohistochemistry images of CD163 and CD206 (A). Immunohistochemistry used to measure the expression of CD163 (B) and CD206 (C). Scale bar, 100 μm. * $p < 0.05$ vs. CSF-1, ** $p < 0.01$ vs. CSF-1, *** $p < 0.001$ vs. CSF-1.

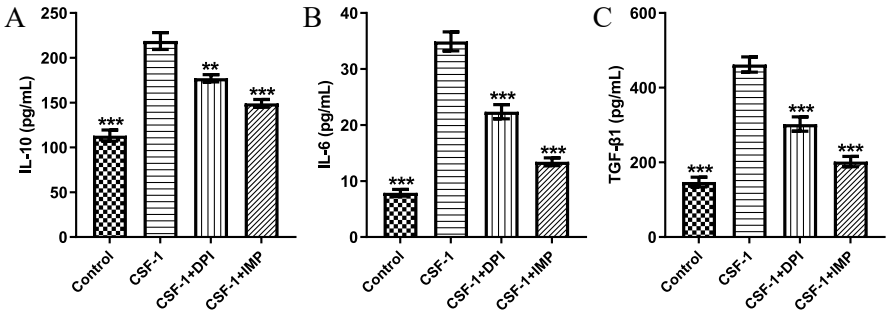

Fig. 3 Effect of IMP (10 μM) on the expression levels of M2 macrophage phenotype markers. ELISA was used to quantify the expression levels of IL-10 (A), IL-6 (B), and TGF-β1 (C). ** $p < 0.01$ vs. CSF-1, *** $p < 0.001$ vs. CSF-1.

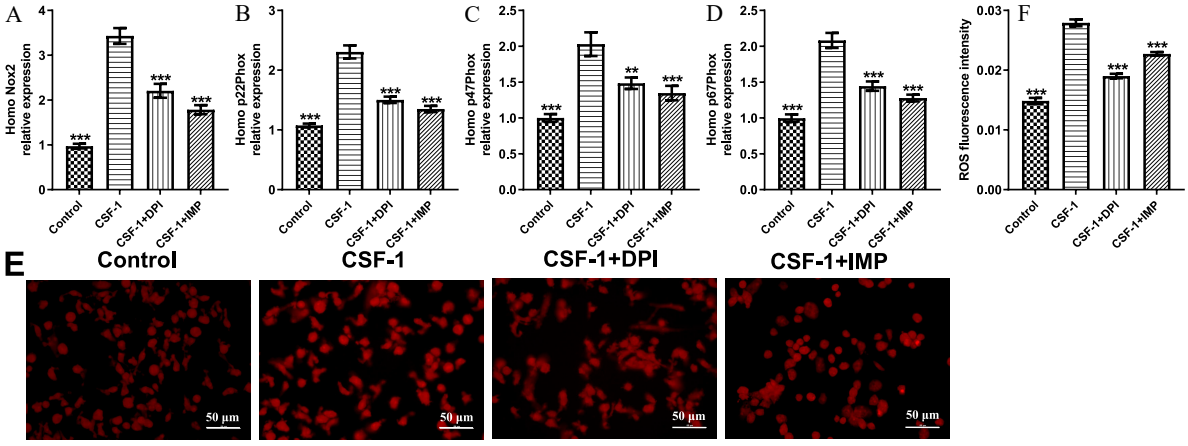

Fig. 4 Effect of IMP (10 μM) on Nox2-associated mRNA and ROS expression. The mRNA protein expression level of Homo Nox2 (A), Homo p22phox (B), Homo p47phox (C), and Homo p67phox (D). The Fluorescence staining images showing the effect of IMP (E) and quantification of ROS levels (F). Scale bar, 50 μm. ** $p < 0.01$ vs. CSF-1, *** $p < 0.001$ vs. CSF-1.

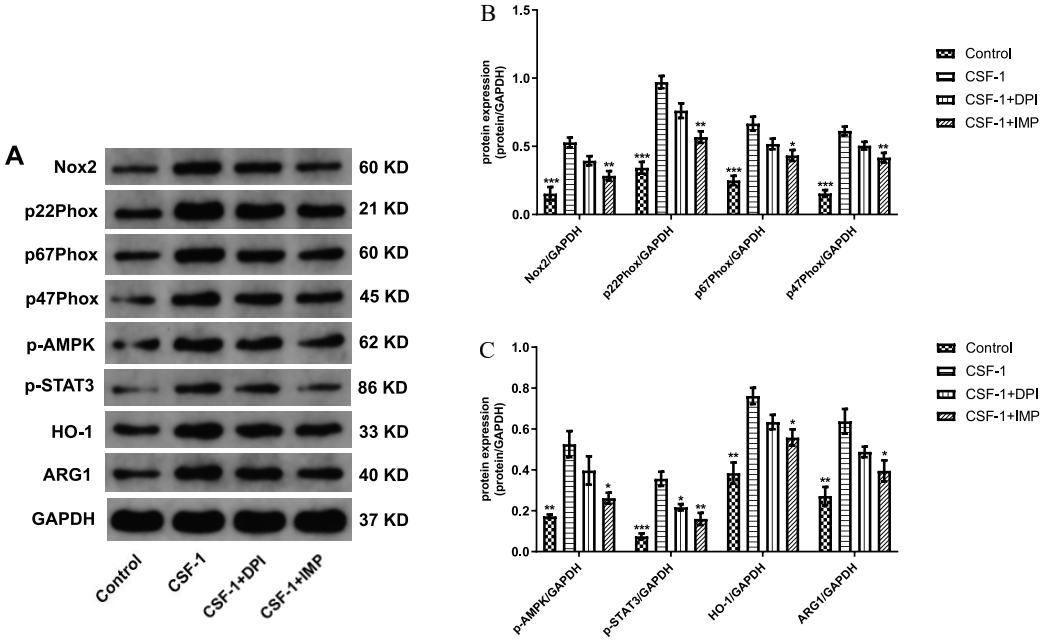

Fig. 5 Effect of IMP (10 μM) on the expression of Nox2/AMPK pathway-associated proteins. Western blot images (A), Western blot analysis used to measure the protein expression level of Nox2, p22phox, p67phox, p47phox (B), and p-AMPK, p-STAT3, HO-1, ARG1 (C). * $p < 0.05$ vs. CSF-1, ** $p < 0.01$ vs. CSF-1, *** $p < 0.001$ vs. CSF-1.

of colon cancer HT-29 and LoVo cells by regulating the Nox2/ROS/AMPK/STAT3 pathway.

In recent years, with the increasing research on TME, immunotherapy has a considerable potential in cancer treatment. TAMs are the major immune cell population in the TME [18]. TAMs play a dual role in modulating inflammation and tumor development. In the early stage of tumors, TAMs create an inflammatory microenvironment that can induce mutations and promote tumor cell proliferation. During tumor progression, TAMs promote angiogenesis, enhance tumor cell migration and invasion, and suppress the antitumor immune response [19]. Increasing evidence has focused on targeting TAM apoptosis and phenotype reversal in the regulation of multiple cancers such as breast cancer [20], making TAMs an important target for cancer immunotherapy. At present, the mechanism underlying the antitumor effect of imperatorin remains unclear. In this study, THP-1 cells were differentiated into macrophages using PMA, treated with CSF-1, and co-cultured with colon cancer HT-29 and LoVo cells. Based on the results of our preliminary experiments, 10 μM imperatorin was selected for experimental intervention. Wu et al [13] used the same concentration in their study and found that this concentration exhibits low general toxicity in human epithelial, ovarian, colon, and non-small cell lung cancer cell lines. In addition, Zheng et al [21] reported that the IC_{50} of IMP in HT-29 cells was 78 μM, and increasing the concentration of IMP did not affect the percentage of necrotic cell death. Therefore, 10 μM IMP is likely to exhibit minimal toxicity in both LoVo and HT-29 cells. A significant reduction in cell viability was observed at 72 h, which may be related to macrophage involvement and a potential time-lag effect. A similar hypothesis was also proposed by Jang et al [22] in a three-dimensional co-culture system of pancreatic cancer. However, this part of the study has certain limitations. To better determine whether the observed decline in cell viability is attributable to the direct cytotoxic effects of IMP or to the influence of macrophage-derived factors, future experiments should include a control group in which HT-29 and LoVo cells are treated with IMP alone, without macrophage-conditioned medium. This would help clarify the respective contributions of direct and macrophage-mediated effects. Our observation indicated that IMP intervention for 72 h reduced the viability of HT-29 and LoVo cells, and this effect may be related to macrophages.

TAMs can be classified into M1 and M2 types. Studies have shown that M1 macrophages are tumor suppressive, pro-inflammatory, and immunoreactive, whereas M2 macrophages are involved in tissue repair, immune escape, and the promotion of tumorigenesis and tumor progression. Infiltration of M2 macrophages in tumors is significantly increased and correlated with poor patient prognosis [23]. Patients with high M2 macrophage infiltration have approximately twice the risk of tumor recurrence and tumor-related mortality compared with those with low M2

infiltration [24]. CSF-1 is an important cytokine correlated with TAM immunosuppressive function. Tumor cells release large amounts of CSF-1 into the extracellular environment during rapid proliferation. CSF-1 acts as a chemoattractant mediating binding to receptors on TAMs and recruiting them to tumor cells, inducing increased fatty acid oxidation (FAO) levels in TAMs and promoting their polarization into M2-phenotype macrophages [25]. The distinctive surface markers of M2 macrophages are CD163 and CD206, and M2 macrophages secrete cytokines and chemokines such as IL-10, IL-6, TGF-β, ARG-1, and H0-1, thereby exerting immunosuppression and accelerating tumor development [26]. In our study, administration with CSF-1 induced the polarization of M0 macrophages into M2 macrophages. Immunohistochemical analysis showed elevated expression levels of the M2 macrophage surface markers CD163 and CD206, and the ELISA results also suggested that the expression of IL-10, IL-6, and TGF-β levels increased in M2 macrophages. Treatment with IMP or the antioxidant DPI significantly downregulated the expression of CD163 and CD206 and reduced the expression of correlated cytokines and chemokines. These findings suggest that both IMP and DPI may play an antitumor role by inhibiting M2 macrophage polarization and regulating TMEs, and the ability of IMP to influence M2 macrophages may be related to ROS.

Compared with normal cells, the TME is always associated with oxidative stress, and the concentration of ROS can be up to 100 times higher than that in normal tissue cells. ROS produced by cancer cells can recruit and support TAMs for tumor growth and prevent T-cell infiltration into tumors. Therefore, regulating ROS levels may represent a potential strategy to modulate the TME and overcome cancer cell drug resistance [27, 28]. Che et al [29] showed that M2 macrophage polarization in colon cancer is largely dependent on ROS, and inhibition of ROS production specifically blocks M2 macrophage polarization and reduces colorectal cancer metastasis. In cells, ROS is mainly derived from the Nox family, and Nox-dependent ROS has been shown to induce M2 polarization in the TME [30]. Nox2-dependent ROS can trigger autophagy, which promotes hepatocellular carcinoma-induced M2 macrophage polarization [10]. In M2 macrophages, Nox2 is the most highly expressed member of the Nox family, and the administration of DPI reduced the expression of Nox2 and ROS [7]. In our study, induction of macrophage polarization to the M2 macrophages by CSF-1 resulted in increased expression of subunits p22phox, p47phox, and p67phox, and Nox2 mRNA is required for Nox2 activation. DHE fluorescent staining showed increased ROS levels in M2 macrophages. Western blot results further confirmed that the protein expression levels of Nox2, p22phox, p47phox, and p67phox were upregulated in M2 macrophages. Treatment with IMP or DPI significantly downregulated oxidative stress in M2 macrophages and reduced ARG-1 and H0-1 expression. These findings suggest that IMP may reduce the oxidative stress in M2 macrophages through the Nox2-ROS pathway, thereby inhibiting M2 macrophage polarization and regulating TAM phenotypic transformation.

We further explored the potential mechanisms underlying macrophage polarization. Previous studies have reported that Nox2 can be regulated by AMPK in the cardiovascular system [31] and that AMPK activation is involved in macrophage polarization [32]. AMPK has been proposed to act as an intermediate regulator of macrophage inflammatory activity, being rapidly activated by anti-inflammatory stimuli and inactivated by pro-inflammatory stimuli. Exposure to anti-inflammatory cytokines such as IL-10 and TGF-β significantly increases AMPK expression and activity, whereas exposure to pro-inflammatory cytokines such as TNF-α and IL-1β reduces them [33]. In addition, AMPK activation has been shown to decrease IκB degradation and increase Akt activation, thereby inhibiting inflammatory responses, suppressing M1 phenotype macrophages, and promoting polarization toward the anti-inflammatory M2 phenotype macrophages [34]. STAT3 transcription factors are recognized as key regulators of inflammatory responses in macrophages and other immune cells [3]. TAM-derived IL-6 has been reported to promote breast cancer development and progression through STAT3 [35]. Besides, activation of the Janus kinase 2 (JAK2)/STAT3 signaling pathway in gastric cancer cells and mouse gastric cancer tissues has been shown to enhance M2 phenotype macrophage polarization, thereby facilitating tumor metastasis and angiogenesis [36]. In addition, inhibition of the STAT3 and AKT signaling pathways in colon cancer downregulates TAM polarization toward the M2 phenotype, resulting in decreased expression of PD-L1 and IL-10 in M2-polarized TAM in the TME [37]. In IL-4 induced M2 macrophage polarization, the phosphorylation levels of both AMPK and STAT3 are significantly elevated, and blockade of either AMPK or STAT3 inhibits M2 macrophage polarization [38]. These data suggest that the anti-inflammatory and antitumor characteristics of the AMPK/STAT3 signaling pathway are associated with M1/M2 polarization of macrophages. In our study, we observed elevated p-AMPK and p-STAT3 expression in M2 macrophages, and administration of IMP or DPI decreased their expression, suggesting that IMP inhibited cancer cell viability by decreasing Nox2/ROS expression, downregulating the AMPK/STAT3 signaling pathway, modulating macrophage polarization, and affecting the TME.

CONCLUSION

Our findings indicate that IMP inhibits M2 macrophage polarization and reduces the proliferative ability of

colon cancer HT-29 and LoVo cells by downregulating the expression of the Nox2/ROS/AMPK/STAT3 signaling pathway. Our results suggest an essential role of IMP in cancer therapy. However, further studies and clinical trials are needed to confirm the effectiveness of IMP in different cancer types. IMP may emerge as a novel therapeutic option for cancer treatment in the future.

Appendix A. Supplementary data

Supplementary data associated with this article can be found at https://dx.doi.org/10.2306/scienceasia1513-1874.2026.004.

Acknowledgements: This work was supported by the Shaanxi Provincial Department of Science and Technology, Natural Science Basic Research Program-Key Project (2025JCQYCX-076); the Key industrial innovation chain project of Shaanxi (Grant No. 2021ZDLSF01-07); the Science and Technology Innovation Quality Improvement and Capacity Expansion Program-TCM Scientific Research and Innovation Talent Project (Grant No. TZKN-CXRC-19); and the Shaanxi Provincial Peoples Hospital Science and Technology Development Incubation Funding (Grant No. 2023YJY-64).

REFERENCES

1. Sung H, Ferlay J, Siegel RL, Laversanne M, Soerjomataram I, Jemal A, Bray F (2021) Global cancer statistics 2020: GLOBOCAN estimates of incidence and mortality worldwide for 36 cancers in 185 countries. *CA Cancer J Clin* **71**, 209–249.
2. Li N, Zhu Q, Tian Y, Ahn KJ, Wang X, Cramer Z, Jou J, Folkert IW, et al (2023) Mapping and modeling human colorectal carcinoma interactions with the tumor microenvironment. *Nat Commun* **14**, 7915.
3. Basak U, Sarkar T, Mukherjee S, Chakraborty S, Dutta A, Dutta S, Nayak D, Kaushik S, et al (2023) Tumor-associated macrophages: An effective player of the tumor microenvironment. *Front Immunol* **14**, 1295257.
4. Xie J, Deng W, Deng X, Liang JY, Tang Y, Huang J, Tang H, Zou Y, et al (2023) Single-cell histone chaperones patterns guide intercellular communication of tumor microenvironment that contribute to breast cancer metastases. *Cancer Cell Int* **23**, 311.
5. Marangon D, Lecca D (2023) Exosomal non-coding RNAs in glioma progression: insights into tumor microenvironment dynamics and therapeutic implications. *Front Cell Dev Biol* **11**, 1275755.
6. Chen Z, Han F, Du Y, Shi H, Zhou W (2023) Hypoxic microenvironment in cancer: molecular mechanisms and therapeutic interventions. *Signal Transduct Target Ther* **8**, 70.
7. Dilly S, Romero M, Solier S, Feron O, Dessy C, Slama Schwok A (2023) Targeting M2 macrophages with a novel NADPH oxidase inhibitor. *Antioxidants* **12**, 440.
8. Bedard K, Krause KH (2007) The NOX family of ROS-generating NADPH oxidases: physiology and pathophysiology. *Physiol Rev* **87**, 245–313.
9. van der Vliet A, Danyal K, Heppner DE (2018) Dual oxidase: A novel therapeutic target in allergic disease. *Br J Pharmacol* **175**, 1401–1418.
10. Shiau DJ, Kuo WT, Davuluri GVN, Shieh CC, Tsai PJ, Chen CC, Lin YS, Wu YZ, et al (2020) Hepatocellular carcinoma-derived high mobility group box 1 triggers M2 macrophage polarization via a TLR2/NOX2/autophagy axis. *Sci Rep* **10**, 13582.
11. Tsai ML, Tsai YG, Lin YC, Hsu YL, Chen YT, Tsai MK, Liao WT, Lin YC, et al (2021) IL-25 induced ROS-mediated M2 macrophage polarization via AMPK-associated mitophagy. *Int J Mol Sci* **23**, 3.
12. Zhou N, Yong S, Shi X, Zhang P, Wang J (2023) Imperatorin derivative OW1, a new vasoactive compound, attenuates cell proliferation and migration by inhibiting Nox1-mediated oxidative stress. *J Pharm Pharmacol* **75**, 502–514.
13. Wu CP, Murakami M, Li YC, Huang YH, Chang YT, Hung TH, Wu YS, Ambudkar SV (2023) Imperatorin restores chemosensitivity of multidrug-resistant cancer cells by antagonizing ABCG2-mediated drug transport. *Pharmaceuticals (Basel)* **16**, 1595.
14. Luo KW, Sun JG, Chan JY, Yang L, Wu SH, Fung KP, Liu FY (2011) Anticancer effects of imperatorin isolated from *Angelica dahurica*: induction of apoptosis in HepG2 cells through both death-receptor- and mitochondria-mediated pathways. *Chemotherapy* **57**, 449–459.
15. Xian Z, Choi YH, Zheng M, Jiang J, Zhao Y, Wang C, Li J, Li Y, et al (2020) Imperatorin alleviates ROS-mediated airway remodeling by targeting the Nrf2/HO-1 signaling pathway. *Biosci Biotechnol Biochem* **84**, 898–910.
16. Yong S, Zhou N, Zhou Y, Zhang X (2023) Imperatorin attenuates the proliferative activity of MKN-45 and HT-29 cells by inhibiting the Noxs-ROS pathway. *Drug Clin* **8**, 1836-184.
17. Liao X, Zhang Z, Ming M, Zhong S, Chen J, Huang Y (2023) Imperatorin exerts antioxidant effects in vascular dementia via the Nrf2 signaling pathway. *Sci Rep* **13**, 5595.
18. Li L, Yang Y, Zhang J, Wang X, Ye Z (2025) FOXP3 influences recruitment and polarization of macrophages via regulating CCL5 in non-small cell lung cancer. *ScienceAsia* **51**, ID 2025021.
19. 10.3389/fimmu.2023.1295684 Shao S, Miao H, Ma W (2023) Unraveling the enigma of tumor-associated macrophages: challenges, innovations, and the path to therapeutic breakthroughs. *Front Immunol* **14**, 1295684.
20. Chen JS, Teng YN, Chen CY, Chen JY (2023) A novel STAT3/NFκB p50 axis regulates stromal-KDM2A to promote M2 macrophage-mediated chemoresistance in breast cancer. *Cancer Cell Int* **23**, 237.
21. Zheng YM, Lu AX, Shen JZ, Kwok AH, Ho WS (2016) Imperatorin exhibits anticancer activities in human colon cancer cells via the caspase cascade. *Oncol Rep* **35**, 1995–2002.
22. Jang SD, Song J, Kim HA, Im CN, Khawar IA, Park JK, Kuh HJ (2021) Anti-cancer activity profiling of chemotherapeutic agents in 3D co-cultures of pancreatic tumor spheroids with cancer-associated fibroblasts and macrophages. *Cancers (Basel)* **13**, 5955.
23. Gu L, Feng C, Li M, Hong Z, Di W, Qiu L (2023) Exosomal NOX1 promotes tumor-associated macrophage M2 polarization-mediated cancer progression by stimulating ROS production in cervical cancer: A preliminary study. *Eur J Med Res* **28**, 323.
24. Waniczek D, Lorenc Z, Śnietura M, Wesecki M, Kopec A, Muc-Wierzgoń M (2017) Tumor-associated macrophages and regulatory T cells infiltration and the clinical out-

come in colorectal cancer. *Arch Immunol Ther Exp* **65**, 445–454.
25. Ruffell B, Coussens LM (2015) Macrophages and therapeutic resistance in cancer. *Cancer Cell* **27**, 462–472.
26. Wu K, Lin K, Li X, Yuan X, Xu P, Ni P, Xu D (2020) Redefining tumor-associated macrophage subpopulations and functions in the tumor microenvironment. *Front Immunol* **11**, 1731.
27. Malla RR, Kamal MA (2021) ROS-responsive nanomedicine: Towards targeting the breast tumor microenvironment. *Curr Med Chem* **28**, 5674–5698.
28. Wang P, Gong Q, Hu J, Li X, Zhang X (2021) Reactive oxygen species (ROS)-responsive prodrugs, probes, and theranostic prodrugs: Applications in the ROS-related diseases. *J Med Chem* **64**, 298–325.
29. Che N, Li M, Liu X, Cui CA, Gong J, Xuan Y (2024) Macelignan prevents colorectal cancer metastasis by inhibiting M2 macrophage polarization. *Phytomedicine* **122**, 155144.
30. Xu Q, Choksi S, Qu J, Jang J, Choe M, Banfi B, Engelhardt JF, Liu ZG (2016) NADPH oxidases are essential for macrophage differentiation. *J Biol Chem* **291**, 20030–20041.
31. Li Y, He B, Zhang C, He Y, Xia T, Zeng C (2023) Naringenin attenuates isoprenaline-induced cardiac hypertrophy by suppressing oxidative stress through the AMPK/NOX2/MAPK signaling pathway. *Nutrients* **15**, 1340.
32. Ye W, Wang J, Lin D, Ding Z (2020) The immunomodulatory role of irisin on osteogenesis via AMPK-mediated macrophage polarization. *Int J Biol Macromol* **146**, 25–35.
33. Cui Y, Chen J, Zhang Z, Shi H, Sun W, Yi Q (2023) The role of AMPK in macrophage metabolism, function and polarisation. *J Transl Med* **21**, 892.
34. Sag D, Carling D, Stout RD, Suttles J (2008) Adenosine 5′-monophosphate-activated protein kinase promotes macrophage polarization to an anti-inflammatory functional phenotype. *J Immunol* **181**, 8633–8641.
35. Radharani NNV, Yadav AS, Nimma R, Kumar TVS, Bulbule A, Chanukuppa V, Kumar D, Patnaik S, et al (2022) Tumor-associated macrophage derived IL-6 enriches cancer stem cell population and promotes breast tumor progression via Stat-3 pathway. *Cancer Cell Int* **22**, 122.
36. Mu G, Zhu Y, Dong Z, Shi L, Deng Y, Li H (2021) Calmodulin 2 facilitates angiogenesis and metastasis of gastric cancer via STAT3/HIF-1A/VEGF-A mediated macrophage polarization. *Front Oncol* **11**, 727306.
37. de Carvalho TG, Lara P, Jorquera-Cordero C, Aragão CFS, de Santana Oliveira A, Garcia VB, de Paiva Souza SV, Schomann T, et al (2023) Inhibition of murine colorectal cancer metastasis by targeting M2-TAM through STAT3/NF-kB/AKT signaling using macrophage 1-derived extracellular vesicles loaded with oxaliplatin, retinoic acid, and *Libidibia ferrea*. *Biomed Pharmacother* **168**, 115663.
38. Kong X, Liu H, Chen F (2017) CaMKKβ promotes mouse macrophage M2 polarization by activating AMPK/JAK2/STAT3 signaling. *J Shanghai Jiao Univ (Med Sci)* **7**, 914–923.

Appendix A. Supplementary data

Table S1 Primer sequences used for RT-PCR.

Gene	Primer	Sequence (5′ − 3′)	PCR product
Homo GAPDH	Forward Reverse	TCAAGAAGGTGGTGAAGCAGG TCAAAGGTGGAGGAGTGGGT	115 bp
Homo Nox2	Forward Reverse	TAAGATAGCGGTTGATGGG TTGAGAATGGATGCGAAGG	114 bp
Homo p22Phox	Forward Reverse	CATTGTGGCGGGCGTGTT CGGCGGTCATGTACTTCTGTC	101 bp
Homo p47Phox	Forward Reverse	TGACGAGACGGAAGACCCTGAG TGGACGGGAAGTAGCCTGTGA	185 bp
Homo P67Phox	Forward Reverse	TTGAAGAAGGGCAATGAT TTTGGAACTAGGAGGAGC	165 bp